Research Article

Yun Sang Shin, Ae Ran Lim* and Jin-Hae Chang*

Influence of diamine structure on the properties of colorless and transparent polyimides

https://doi.org/10.1515/rams-2025-0190
Received August 17, 2025; accepted November 30, 2025;
published online December 17, 2025

Abstract: Nine poly(amic acid)s (PAAs) were synthesized by reacting butane-1,4-diyl bis(1,3-dioxo-1,3-dihydroisobenzofuran-5-carboxylate) dianhydride with various diamine monomers, including *m*-xylylenediamine, *p*-xylylenediamine, 4,4′-oxydianiline, bis(3-aminophenyl) sulfone, bis[4-(3-aminophenoxy)phenyl] sulfone, 2,2′-bis(trifluoromethyl)benzidine, *N*,*N*′-[2,2′-bis(trifluoromethyl)-4,4′-biphenylene]bis(3-aminobenzamide), 2,2-bis[4-(4-aminophenoxy)phenyl]propane, and 2,2-bis[4-(4-aminophenoxy)phenyl]hexafluoropropane. These PAAs were subsequently converted into colorless and transparent polyimide (CPI) films via thermal imidization under various heat treatment conditions. To achieve CPI films with suppressed charge transfer complex formation, the selected diamine monomers featured bent molecular structures, strong electron-withdrawing substituents such as $–CF_3$ or $–SO_2–$, or ether/ketone functional groups incorporated within the backbone. The thermomechanical properties, optical transparency, and solubility of the resulting CPI films were systematically evaluated, and the structure–property relationships between the monomers and CPI film performance were elucidated. Overall, CPI films derived from aromatic or linear main-chain structures exhibited excellent thermal and mechanical properties. In contrast, films incorporating bent structures with polar functional groups or electron-withdrawing substituents in the main chain showed superior optical transparency and solubility.

Keywords: diamine monomer; property; colorless transparent polyimide

***Corresponding authors: Ae Ran Lim**, Department of Science Education, Jeonju University, Jeonju 55069, Republic of Korea, E-mail: arlim@jj.ac.kr; and **Jin-Hae Chang**, Institute of Carbon Technology, Jeonju University, Jeonju 55069, Republic of Korea, E-mail: jhchang@jj.ac.kr
Yun Sang Shin, Department of Science Education, Jeonju University, Jeonju 55069, Republic of Korea

1 Introduction

Polyimides (PIs) and PI-based composites have long been recognized for their exceptional thermomechanical properties, chemical resistance, and, in some cases, optical transparency. These materials have been widely utilized in high-performance applications across various industries, including aerospace, electronics, and automotive sectors [1, 2]. Aromatic PIs, in particular, are known for their excellent thermal stability and flexibility, making them indispensable in the manufacturing of electronic devices and solar panels [3–5]. Furthermore, flexible PI composites have shown significant promise in emerging fields such as electromagnetic interference (EMI) shielding and mechano-electronics [6].

Despite these numerous advantages, conventional PIs typically exhibit a dark brown color due to the formation of charge transfer complexes (CTCs) between polymer chains. This inherent coloration significantly limits their use in optoelectronic applications, particularly in flexible displays, where high optical transparency is essential [7–9].

To develop colorless and transparent polyimides (CPIs), several strategies have been employed to suppress CTC formation: 1. Incorporating bent monomers in *ortho*- (*o*-) or *meta*- (*m*-) configurations to disrupt chain linearity [10, 11]. 2. Introducing bulky substituents into the polymer backbone to inhibit molecular stacking and π-electron delocalization [12, 13]. 3. Using strong electron-withdrawing groups such as trifluoromethyl ($–CF_3$) and hexafluoroisopropylidene ($–C(CF_3)_2–$) to reduce π–π interactions [14–16]. 4. Incorporating flexible ether (–O–), sulfone ($–SO_2–$), or ketone linkages to increase chain mobility [17–19]. 5. Employing cycloaliphatic monomers devoid of π-electrons to enhance transparency [20–22]. Although CPIs derived from cycloaliphatic monomers offer superior solubility, lower dielectric constants, and higher optical transparency than aromatic CPIs, they often suffer from diminished thermal and mechanical performance due to weakened interchain interactions and reduced resonance stabilization [23, 24].

Recently, CPIs have found increasing use not only in display technologies but also in semiconductor packaging, where low weight and high dimensional stability are required [25]. Additionally, CPIs are being explored as

flexible, lightweight plastic substrates to replace traditional glass in advanced electronic devices. In contrast to indium tin oxide (ITO) glass, which is expensive and brittle due to its indium content and rigidity, CPI films offer high thermal stability, excellent optical transmittance, and mechanical flexibility – making them ideal candidates for next-generation bendable, rollable, and wearable electronics [26]. Glass materials also present challenges in high-temperature processes due to their brittleness and thermal shock sensitivity. In comparison, CPI offers processability, lightweight characteristics, and comparable or superior performance [27, 28].

Most CPIs developed to date have utilized rigid aromatic monomers to ensure thermal and mechanical robustness [29]. However, such structures often result in poor solubility and limited processability due to strong π–π interactions and rigidity. Moreover, aromatic components absorb significantly in the visible spectrum, leading to undesirable coloration in the resulting films.

In this study, we employed butane-1,4-diyl bis(1,3-dioxo-1,3-dihydroisobenzofuran-5-carboxylate) (BU-DA), a novel dianhydride containing a flexible aliphatic segment between aromatic rings, as the core dianhydride monomer. The flexibility of BU-DA helps reduce main-chain rigidity and suppress CTC formation. Nine diamine monomers were selected based on their potential to yield CPI characteristics due to the presence of flexible alkyl and ether groups or strong electron-withdrawing substituents such as $–CF_3$ and $(–C(CF_3)_2–)$. Some diamines featured fully bent *m*-configurations, while others had linear backbones with pendant alkyl substituents.

CPI films were synthesized via thermal imidization of the resulting poly(amic acid) (PAA) precursors. The nine diamines used in this work were *m*-xylylenediamine (*m*-XDA), *p*-xylylenediamine (*p*-XDA), 4,4′-oxydianiline (4,4′-ODA), bis(3-aminophenyl) sulfone (*m*-APS), bis[4-(3-aminophenoxy) phenyl] sulfone (*m*-BAPS), 2,2′-bis(trifluoromethyl)benzidine (TFB), N,N′-[2,2′-bis(trifluoromethyl)-4,4′-biphenylene]bis(3-aminobenzamide) (*m*-TFAB), 2,2-bis[4-(4-amino-phenoxy) phenyl]propane (BAPP), and 2,2-bis[4-(4-aminophenoxy) phenyl]hexafluoropropane (6FBAPP). A series of CPI films were fabricated, and their thermomechanical properties, solubility, and optical transparency were thoroughly investigated.

The objective of this study was to optimize reaction conditions for the synthesis of CPIs and to elucidate the relationships between the molecular structures of the diamine monomers and the physical properties of the resulting CPI films. Special attention was given to analyzing the effects of diamine structure on CTC formation and its influence on optical transparency and other key performance metrics.

2 Experimental

2.1 Materials

Butane-1,4-diyl bis(1,3-dioxo-1,3-dihydroisobenzofuran-5-carboxylate) (BU-DA) was obtained from Lum. Tech. Co. (Taipei, Taiwan). (The nine diamine monomers – m-XDA, *p*-XDA), 4,4′-ODA, *m*-APS, *m*-BAPS, TFB, *m*-TFAB, BAPP, and 6FBAPP – were purchased from TCI (Tokyo, Japan) and used without further purification. *N,N′*-Dimethylacetamide (DMAc), purchased from Sigma-Aldrich (Yongin, Korea), was dried thoroughly to remove moisture before use.

2.2 Synthesis of CPI Films

Scheme 1 illustrates the synthesis route of CPI films via a two-step process involving PAA formation followed by thermal imidization. As the procedures for all nine diamine monomers were essentially identical, the synthesis using *m*-XDA is described here as a representative example: BU-DA (5.698 g, 1.3×10^{-2} mol) was completely dissolved in 50 mL of dried DMAc under stirring for 30 min. Then, *m*-XDA (1.770 g, 1.3×10^{-2} mol) was added to the BU-DA solution, and the mixture was stirred at 0 °C under a nitrogen atmosphere for 1 h. The solution was then polymerized at room temperature for 14 h to form the PAA precursor.

The resulting PAA solution was cast uniformly onto a clean glass plate, followed by vacuum stabilization at 50 °C for 1 h. The solvent was then gradually removed under vacuum at 80 °C for an additional hour. The PAA film was subsequently thermally imidized at various temperatures under a nitrogen atmosphere, with specific thermal treatment conditions summarized in Table 1. After thermal imidization, the resulting CPI film was immersed in a 5 wt% aqueous hydrofluoric acid (HF) solution to detach it from the glass substrate. The final freestanding CPI films were obtained with dimensions up to 10×10 cm^2.

2.3 Characterization

Fourier-transform infrared (FT-IR) spectroscopy (PerkinElmer, L-300, London, UK) was used to confirm the imidization of CPI by identifying characteristic functional groups in the range of 4,000–1,000 cm^{-1}.

The ^{1}H and ^{13}C magic angle spinning (MAS) nuclear magnetic resonance (NMR) spectra were recorded at 850 MHz and 125.75 MHz, respectively, on a Bruker spectrometer (Germany) at the Laboratory of NMR, NCIRF, Seoul National University. The ^{1}H and ^{13}C chemical shifts were

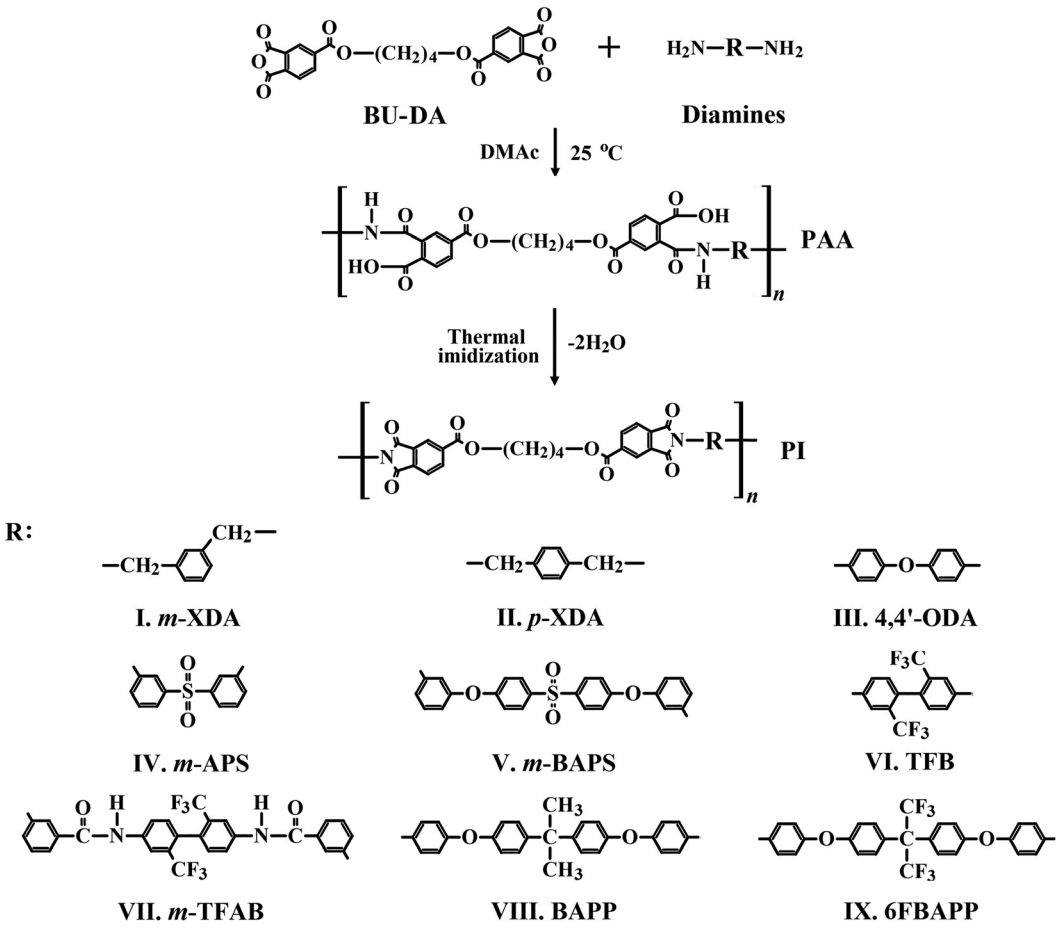

Scheme 1: Synthetic routes for CPIs based on BU-DA monomer.

Table 1: Heat treatment conditions of CPIs based on BU-DA monomer.

Sample	Temperature (°C)/time (h)/pressure (Torr)
PAA	0/1/760 → 25/14/760 → 50/1/1 → 80/1/1
CPI	110/0.5/760 → 140/0.5/760 → 170/0.5/760 → 200/0.5/760 → 230/0.5/760 → 250/0.5/760

referenced to tetramethylsilane (TMS), and the ^{1}H NMR experiment was performed using $CDCl_3$ as the solvent.

Differential scanning calorimetry (DSC, NETZSCH 200F3, Berlin, Germany), thermogravimetric analysis (TGA), and derivative thermogravimetry (DTG) (TA Instruments Q-500, New Castle, USA) were performed under a nitrogen atmosphere with heating and cooling rates of 10 °C min^{-1}. The coefficient of thermal expansion (CTE) was measured using a thermomechanical analyzer (TMA, TA Instruments TMA2940, Seiko, Tokyo, Japan) under a constant load of 0.1 N and a heating rate of 10 °C min^{-1}.

Tensile properties were evaluated using a universal testing machine (UTM, Shimadzu AG-50KNX, Japan) with a crosshead speed of 5.00 mm min^{-1}. Each film was tested at least ten times. Outliers were excluded from the dataset, and the average of the remaining values was reported. Experimental error margins were maintained within ±1 MPa for tensile strength and ±0.05 GPa for initial modulus.

The yellowness index (YI) was measured using a spectrophotometer (KONICA MINOLTA CM-3600d, Tokyo, Japan). Ultraviolet–visible (UV–vis) spectroscopy (SHIMADZU UV-3600, Tokyo, Japan) was used to determine the cut-off wavelength (λ_0) and optical transmittance at 500 nm (500 nm^{trans}). To ensure consistency, all CPI films were prepared with a uniform thickness of 42–46 μm.

3 Results and discussion

3.1 FT-IR, ^{13}C MAS NMR, and ^{1}H NMR, analysis

CPIs were synthesized from a single dianhydride, BU-DA, and nine different diamine monomers, as illustrated in Scheme 1. FT-IR spectra of the resulting CPI films are presented in Figure 1. A separate inset was incorporated into

Figure 1 to provide a more detailed view of the spectral range between 2000 and 1,300 cm^{-1}. The absorption bands observed at 3,050–2,874 cm^{-1} correspond to the C–H stretching vibrations originating from aliphatic and aromatic moieties, reflecting the structural characteristics of the aliphatic and aromatic rings within the main chain. In addition, the strong absorption peaks appearing at 1783–1780 cm^{-1} and 1717–1704 cm^{-1} are assigned to the characteristic C=O stretching vibrations of the imide ring, corresponding to the asymmetric and symmetric modes, respectively. The peaks in the range of 1,500–1,420 cm^{-1} are attributed to the C=C stretching vibrations of the aromatic rings, indicating that the synthesized polymers retain the aromatic backbone structure. Finally, the absorptions observed at 1,385–1,364 cm^{-1} are assigned to the C–N–C stretching vibrations within the imide ring, which represent a typical characteristic band confirming the formation of polyimide. These results clearly demonstrate that the synthesized CPI films possess the intended chemical structure and that successful cyclization reactions were achieved in all compositions [30].

Further confirmation of successful CPI formation was obtained by solid-state ^{13}C MAS NMR analysis. Representative spectra of CPI structures I, IV, and VII are shown in Figure 2. In structure I, both the ester carbon (a) and imide carbon (b) were observed at 166.03 ppm. Aromatic ring carbons (c, d, e) appeared at 135.68, 129.65, and 124.56 ppm, respectively. The carbon of the alkyl group adjacent to the ester oxygen (f) was found at 66.45 ppm, while the central aliphatic methylene group (h) appeared at 26.77 ppm. The methylene group adjacent to the aromatic ring (g) gave a signal at 42.18 ppm. These results, along with the FT-IR data, confirm the successful synthesis of the CPI structures [31]. The full NMR spectra of structures IV and VII are provided in the Supplementary Figure I.

Among the nine synthesized CPIs, the ^{1}H NMR spectrum of Structure I (Figure 3) shows proton (^{1}H) signals consistent with the proposed CPI structure, while the spectra of the remaining CPIs are provided in Supplementary Figure II. The aromatic protons adjacent to the imide ring (a) appeared at 7.1–8.5 ppm due to the strong deshielding effect of the

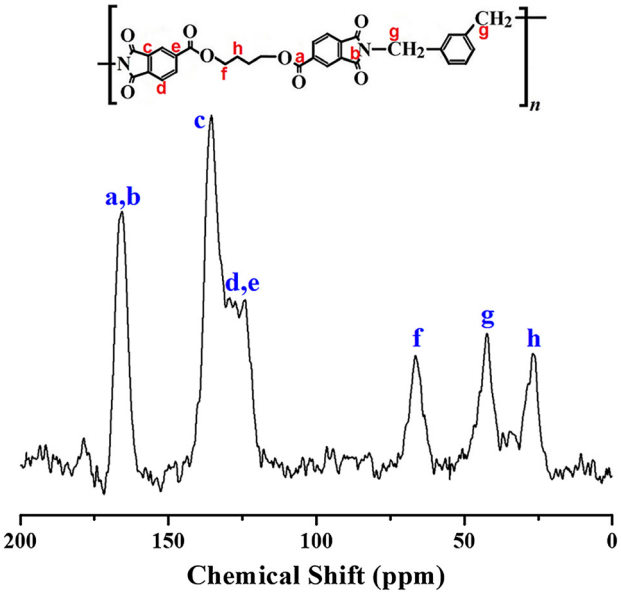

Figure 2: ^{13}C NMR spectrum of structure I based on BU-DA monomer.

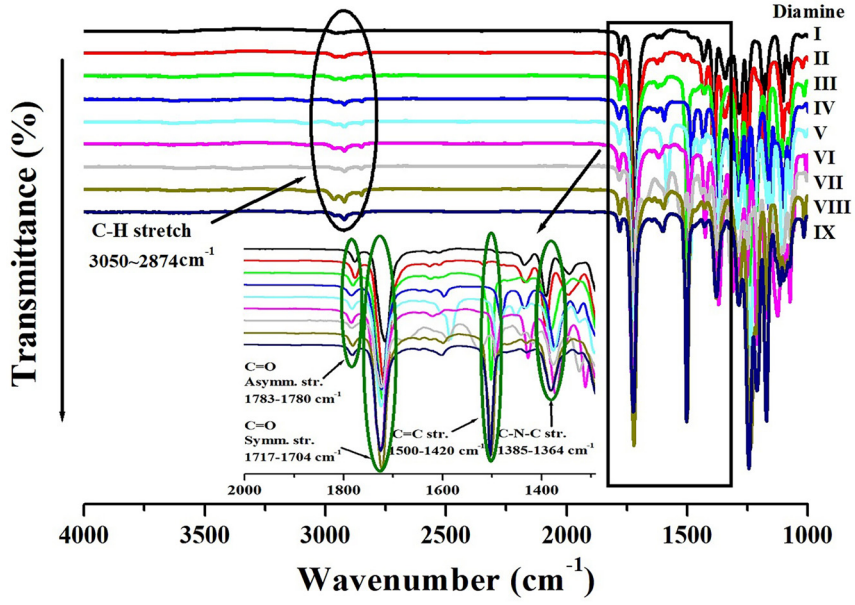

Figure 1: FT-IR spectra of various CPIs based on BU-DA monomer.

carbonyl groups. The methylene protons bonded to the imide nitrogen (b) were observed at 4.7–4.9 ppm, reflecting the influence of the electronegative nitrogen and neighboring carbonyls. The protons adjacent to oxygen or carbonyl groups (c) resonated at 4.3–4.6 ppm. Finally, the aliphatic protons (d) appeared as broad multiplets at 1.5–2.2 ppm, consistent with shielding in the aliphatic environment. These assignments confirm that the proton environments are in good agreement with the designed CPI structure [31].

3.2 Thermal properties

Since CPI is generally amorphous, it does not exhibit a melting point (T_m) detectable by DSC [32]. Instead, the primary thermal characteristic of interest is the glass transition temperature (T_g), which is highly sensitive to monomer structure, chain flexibility, bulky substituents, free volume, and inter- and intramolecular interactions such as hydrogen bonding [33].

The measured T_g values of the nine CPI films are summarized in Table 2, and their proposed 3D polymer structures are illustrated in Figure 4. CPI structures I and II showed the lowest T_g values (112 °C and 130 °C, respectively), attributed to the presence of flexible alkyl groups and the bent *m*-substitution in structure I. Structure III, containing an ether linkage allowing free rotation, exhibited a slightly higher T_g of 146 °C. The relatively low T_g values of structures I–III may also be due to their lower aromatic content, resulting in reduced rigidity.

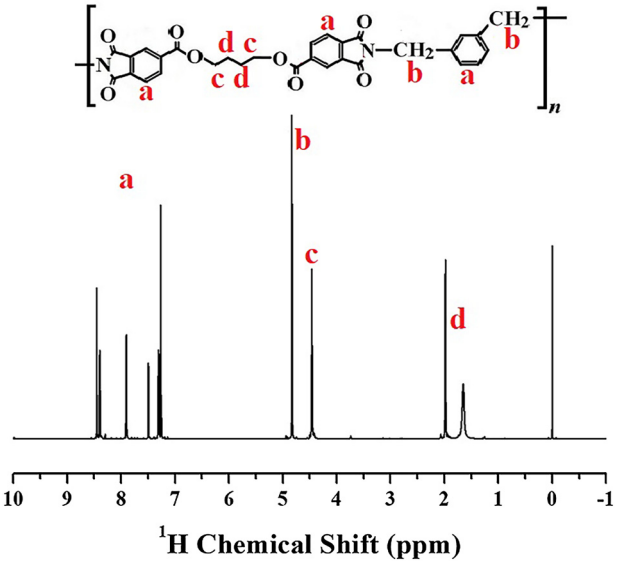

Figure 3: ^{1}H NMR spectrum of structure I based on BU-DA monomer.

Table 2: Thermal properties of CPIs based on BU-DA monomer.

Diamine	T_g (°C)	T_D^{ia} (°C)	wt_R^{600b} (%)	CTE^c (ppm/°C)
I	112	346	37	57.7
II	130	368	36	55.7
III	146	365	59	52.9
IV	149	367	59	49.0
V	157	370	48	48.6
VI	165	370	55	56.3
VII	171	378	61	52.1
VIII	154	382	64	56.6
IX	160	379	48	58.8

[a]Initial decomposition temperature at 2 % weight loss. [b]Weight residue at 600 °C. [c]Coefficient of thermal expansion for 2nd heating is 30~100 °C.

Structures IV and V, which incorporate the bulky and electron-withdrawing –SO_2– group, showed T_g values of 149 °C and 157 °C, respectively. The presence of sulfone groups introduces steric hindrance that restricts segmental motion. The higher T_g of structure V compared to structure IV is attributed to its increased aromatic content. Structures VI, VII, and IX exhibited relatively high T_g values (160–171 °C) due to reduced segmental mobility from the bulky –CF_3 substituents [34, 35]. Structure VII showed the highest T_g (171 °C), likely due to the presence of amide groups capable of forming intermolecular hydrogen bonds, which further restrict chain motion and increase the thermal energy required for transition [36, 37]. In contrast, structure VIII displayed a comparatively lower T_g (154 °C), despite its bulky substituents, because of the flexibility imparted by alkyl groups [38]. In the case of CPIs, the T_g is generally lower compared to that of conventional aromatic PIs. This tendency can be attributed to the specific structural modifications introduced to suppress CTC formation, which is essential for achieving optical transparency. For instance, the incorporation of flexible linkages such as ether bonds (–O–) or bulky substituents including –CF_3 and –$C(CF_3)_2$– not only reduces intermolecular interactions but also decreases chain rigidity. These structural features increase the free volume and enhance segmental mobility, thereby lowering the thermal energy required for the glass transition. Consequently, while CPIs exhibit excellent optical transparency by minimizing intermolecular electronic interactions, this design strategy inevitably compromises chain stiffness, leading to a reduced T_g relative to traditional aromatic polyimides [39, 40]. Figure 5 displays the DSC thermograms of the CPI films.

Thermal stability was further assessed using thermogravimetric analysis (TGA), and the initial decomposition temperatures (T_D^i) and residual weights at 600 °C (wt_R^{600}) are summarized in Table 2 and shown in Figure 6. T_D^i values ranged from 346 °C to 382 °C. Structure I exhibited the lowest

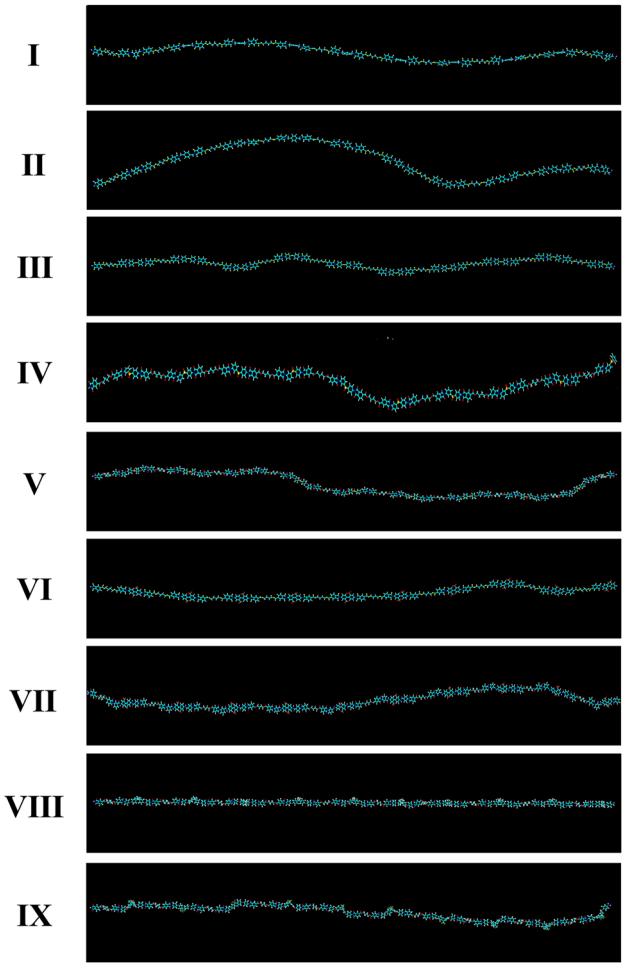

Figure 4: Comparison of the CPI three-dimensional chemical structures based on BU-DA monomer.

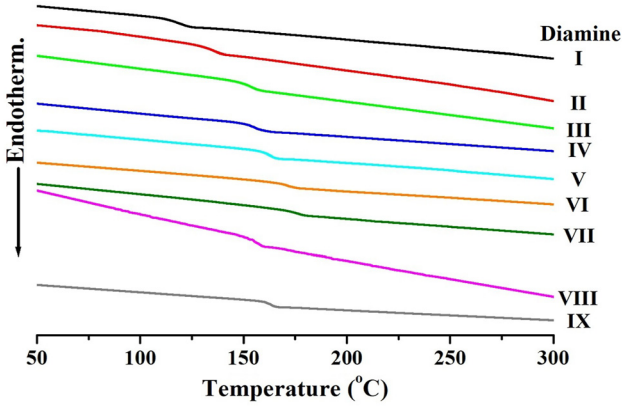

Figure 5: DSC thermograms of various CPIs based on BU-DA monomer.

$T_D{}^i$ (346 °C), likely due to the thermally unstable *m*-linked alkyl chains [41]. Structures II to IV, with para-(*p*-) alkyl, ether, and *m*-sulfone linkages, respectively, showed moderate stability ($T_D{}^i$ = 365–368 °C), attributed to bent

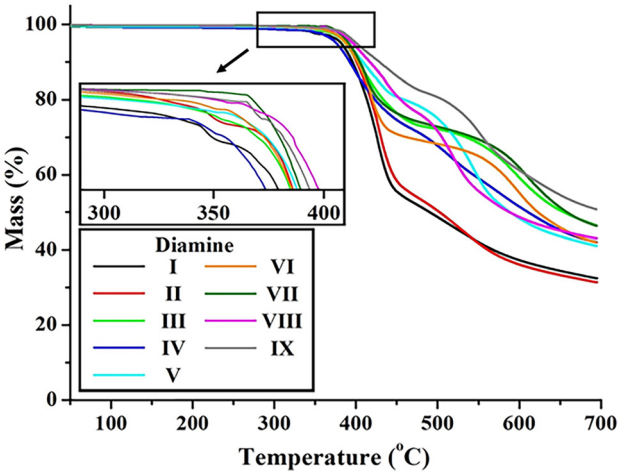

Figure 6: TGA thermograms of various CPIs based on BU-DA monomer.

configurations that limit close chain packing and intermolecular interactions.

Structures V–IX, which feature thermally robust benzene rings and fluorinated substituents, exhibited higher $T_D{}^i$ values (370–382 °C), indicating improved thermal stability [42]. Their linear configurations promote effective molecular packing and reinforce interchain interactions, enhancing thermal endurance [43]. The reason why the $T_D{}^i$ of CPIs is lower than that of conventional aromatic polyimides is primarily related to the structural modifications introduced to suppress CTC formation. While these modifications improve optical transparency, they inevitably weaken the intermolecular interactions that typically enhance thermal stability. Moreover, the incorporation of flexible ether linkages, alkyl substituents, and bulky moieties such as $-CF_3$ reduces the overall bond dissociation energy of the polymer backbone, thereby creating thermally weaker sites that promote earlier thermal degradation. In addition, the increased free volume generated by bulky substituents decreases chain packing density, rendering the polymer matrix more susceptible to the onset of decomposition. Consequently, CPIs exhibit a lower $T_D{}^i$ compared to traditional polyimides, despite maintaining sufficient thermal stability for practical applications. Residual weights at 600 °C ($wt_R{}^{600}$) for these structures generally ranged between 50 % and 64 %, whereas structures I and II, which included thermally labile alkyl groups, showed significantly lower residue values (36–37 %).

DTG analysis provides the rate of weight loss as a function of temperature, thereby offering more detailed insight into the thermal degradation behavior than TGA alone. In particular, for CPIs exhibiting multi-step degradation, the DTG curves clearly reveal the maximum degradation rate temperature (T_{max}) for each stage, which can be correlated with the decomposition of specific structural

units such as imide, ether, or sulfone moieties. Furthermore, DTG enables precise identification of the onset (T_{onset}) and termination (Tend) of degradation, allowing a direct comparison of how additives, fillers, or copolymer compositions affect the decomposition process. Figure 7 shows the DTG curves of nine CPI films prepared from different diamines. All samples exhibited major degradation peaks in the range of 450–550 °C, which are associated with the thermal decomposition of the imide rings and aromatic backbones. However, the position and intensity of the T_{max} varied depending on the diamine structure. CPIs containing rigid aromatic units or strongly electron-withdrawing substituents displayed higher T_{max} values, reflecting enhanced thermal stability. In contrast, CPIs incorporating more flexible chain segments exhibited relatively lower T_{max}, indicating reduced resistance to thermal decomposition. These results demonstrate that DTG analysis provides more detailed information on the stepwise degradation behavior compared with TGA alone, enabling clear identification of structural effects on the thermal stability of CPI films. The TGA/DTG results of the CPI films prepared with various diamines were provided in Supplementary Figure III.

Thermal dimensional stability was evaluated using thermomechanical analysis (TMA). The coefficient of thermal expansion (CTE), which reflects the polymer's tendency to expand upon heating, is sensitive to chain rigidity and aromatic content [44, 45]. Figure 8 and Table 2 show the TMA results. Structures I and II exhibited high CTE values (55.7 and 57.7 ppm °C^{-1}, respectively), due to flexible alkyl content and bent backbones. In contrast, structures IV and V, despite their non-linear chains, showed lower CTE values (48.6 and 49.0 ppm °C^{-1}), attributed to the restricted rotation imparted by the –SO_2– moieties. Among the fluorinated structures (VI–IX), structure VII displayed a relatively low CTE

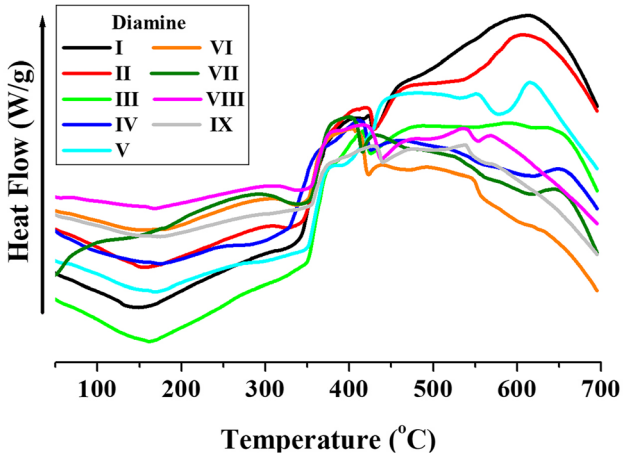

Figure 7: DTG thermograms of various CPIs based on BU-DA monomer.

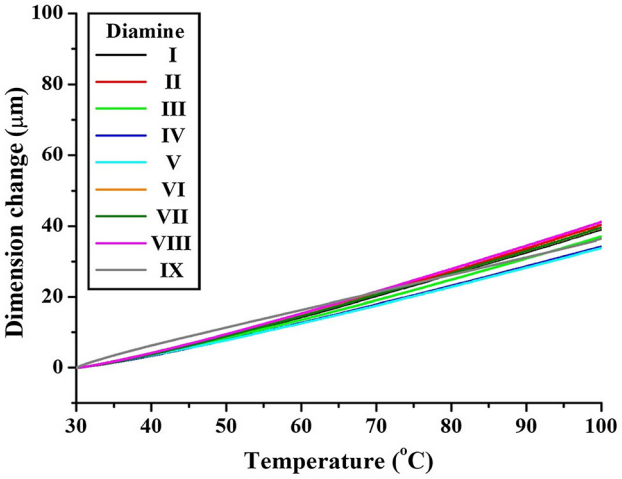

Figure 8: TMA thermograms of various CPIs based on BU-DA monomer.

(52.1 ppm °C^{-1}), due to the potential formation of hydrogen bonds via the –NH–CO– groups. Structure IX exhibited the highest CTE (58.8 ppm °C^{-1}), which can be explained by the flexible hexafluoropropyl (–$C(CF_3)_2$–) substituents, allowing greater chain movement.

3.3 Mechanical properties

The mechanical properties of the CPI films – including ultimate tensile strength, initial modulus, and elongation at break (EB) – were evaluated using a UTM. The results are summarized in Table 3.

Structures I–III exhibited moderate tensile strengths ranging from 54 to 63 MPa. Structure IV, which incorporates a bulky –SO_2– group and a *m*-substitution, displayed the lowest tensile strength (22 MPa) among all samples. This significant reduction in strength is attributed to its highly bent conformation, which limits effective chain alignment (Figure 4). Conversely, although Structure V also contains a –SO_2– moiety,

Table 3: Mechanical properties of CPIs based on BU-DA monomer.

Diamine	Ult. Str.[a] (MPa)	Ini. Mod.[b] (GPa)	E.B.[c] (%)
I	63	6.81	4
II	61	3.09	7
III	54	2.57	6
IV	22	2.23	4
V	57	2.63	4
VI	136	5.96	7
VII	92	2.87	7
VIII	95	4.71	10
IX	95	4.27	9

[a]Ultimate tensile strength. [b]Initial tensile modulus. [c]Elongation at break.

its more linear geometry, facilitated by ether linkages and a higher benzene content, led to a considerably higher tensile strength of 57 MPa. Structures VI–IX demonstrated superior tensile strength values (92–136 MPa), which can be attributed to their relatively linear chain configurations and higher aromatic content. In particular, Structure VI, derived from a simple *p*-substituted diamine, exhibited the highest tensile strength (136 MPa), attributed to its highly regular and linear 3D molecular conformation that enables effective chain packing.

The initial modulus, reflecting the stiffness of the polymer chain, was strongly influenced by structural rigidity and the presence of rigid aromatic units. As shown in Figure 4, Structure I exhibited the highest modulus (6.81 GPa), likely due to its relatively short and linear backbone. Structures VI, VIII, and IX also showed high modulus values (4.27–5.96 GPa), consistent with their more linear architectures. Although Structure VII exhibited a relatively high tensile strength (92 MPa), its modulus was comparatively lower (2.87 GPa), likely due to its overall bent chain configuration, which reduces stiffness despite the presence of hydrogen bonding interactions via amide linkages.

Overall, Structures VI–IX displayed enhanced mechanical performance, with high tensile strength and stiffness, which can be attributed to tightly packed, linear chains, short repeating units, and intermolecular attractions such as hydrogen bonding [46, 47].

The elongation at break (EB) values for all CPI films ranged consistently from approximately 4 %–10 %, suggesting comparable flexibility across the different structures. The reason why CPIs generally exhibit lower EB compared to conventional aromatic PIs can be attributed to their inherent structural characteristics. To suppress CTC formation and achieve optical transparency, CPIs are often designed with bulky substituents such as $-CF_3$, $-C(CF_3)_2-$, or $-SO_2-$ groups, which increase chain rigidity and restrict molecular flexibility. This enhanced rigidity limits the ability of polymer chains to undergo plastic deformation during stretching, leading to brittle fracture and a reduced EB. Furthermore, the incorporation of bulky moieties increases free volume and disrupts uniform chain packing, which facilitates localized stress concentration rather than homogeneous chain extension under load. As a consequence, while CPIs maintain excellent thermal stability and optical transparency, they inevitably suffer from lower ductility, as reflected in their reduced EB [40, 48].

3.4 Optical transparency

To evaluate the optical transparency of the CPI films, three key parameters were measured: the λ_0, the 500 nm^{trans}, and the YI. These values reflect the UV absorption onset, visible light transmittance, and visual coloration of the films, respectively [49]. All films were fabricated with a uniform thickness of 42–46 μm to ensure consistent optical comparison.

UV–vis spectra of the CPI films are shown in Figure 9, and the corresponding data are presented in Table 4. The λ_0 values ranged from 328 to 392 nm depending on the diamine monomer used. Structures III, VIII, and IX exhibited relatively high λ_0 values of 381, 392, and 374 nm, respectively. These results suggest increased CTC formation due to their more linear chain conformations. As a consequence, their 500 nm^{trans} values were slightly lower (81–83 %) compared to the other films. Nevertheless, all films demonstrated visible light transmittance greater than 80 % at 500 nm and transmitted light starting below 400 nm, indicating excellent overall optical transparency.

Table 4 summarizes the YI values, which were calculated using the ASTM E313-96 and DIN 6167 standards with the equation:

$$YI = 100 \times (aX - bZ)/Y$$

where a and b are constants specific to each method, and X, Y, and Z are the tristimulus values.

Structures I and II exhibited the lowest YI values (both < 1), due to their bent, flexible chain structures, which hinder close chain stacking and CTC formation. Structures IV–VII also showed good optical clarity (YI = 2.2–4.2), attributed to structural distortion and *m*-substitution effects.

Notably, although Structure VI contains a linear *p*-substitution, its incorporation of the strongly electron-withdrawing $-CF_3$ group disrupts π-electron delocalization, thereby reducing CTC and lowering YI. In contrast, Structure III retained a relatively linear structure and displayed a significantly higher YI of 19.3. Structures VIII and IX, due to

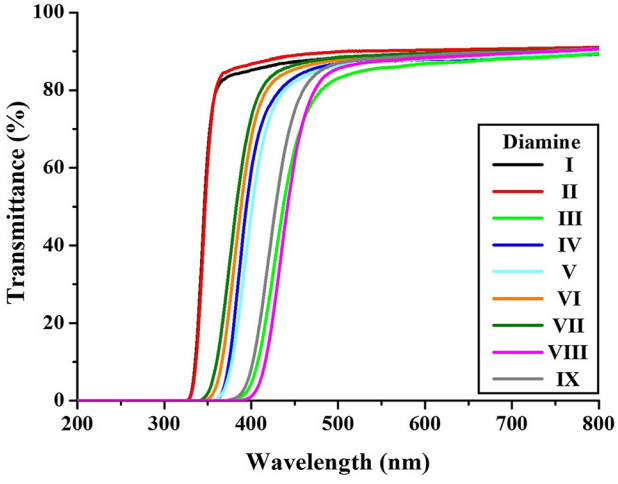

Figure 9: UV–vis. transmittance of various CPIs based on BU-DA monomer.

Table 4: Optical properties of CPIs based on BU-DA monomer.

Diamine	Thickness[a] (μm)	λ_0[b] (nm)	500nm[trans] (%)	YI[c]
I	42	328	88	<1 (0.1)
II	43	328	89	<1 (0.2)
III	42	381	83	19.3
IV	44	360	86	4.2
V	44	358	86	3.6
VI	45	349	87	2.6
VII	46	343	88	2.2
VIII	45	392	81	27.5
IX	46	374	82	15.7

[a]Film thickness. [b]Cut off wavelength. [c]Yellow index.

their linear conformations and lack of significant structural distortion, exhibited the highest YI values (27.5 and 15.7, respectively), consistent with increased coloration resulting from CTC formation.

To visually assess transparency, Figure 10 shows images of a printed logo viewed through each CPI film. Despite color variations due to different monomer structures, all films maintained sufficient clarity for easy logo recognition. These differences are consistent with the measured YI values.

3.5 Solubility

Although CPI materials are known for their excellent thermal and chemical stability, their rigid aromatic backbones often lead to poor solubility in conventional solvents [50, 51]. This limitation restricts their processability and application as high-performance polymer films. Therefore, structural modifications that improve solubility without compromising CPI's desirable properties are of great interest.

In this study, solubility tests were conducted using 12 common solvents, and the results are compiled in Table 5. All CPI films were completely insoluble in polar protic solvents such as ethanol (EtOH) and methanol (MeOH), and only exhibited limited solubility in acetone, dimethyl sulfoxide (DMSO), and toluene. However, higher solubility was observed in halogenated solvents such as chloroform ($CHCl_3$)

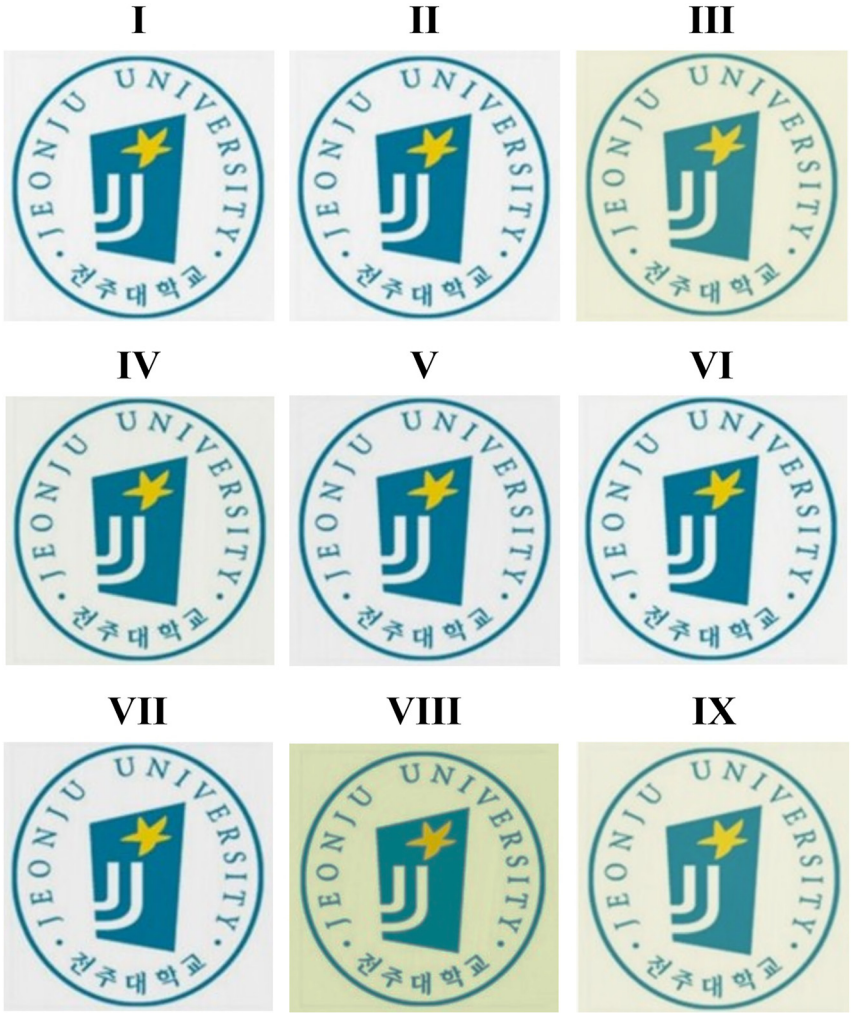

Figure 10: Photographs of various CPIs based on BU-DA monomer.

Table 5: Solubility tests of CPIs based on BU-DA monomer.

Diamine	Act	$CHCl_3$	CH_2Cl_2	DMAc	DMF	DMSO	MeOH	EtOH	NMP	Py	THF	Tol
I	×	◎	◎	×	△	×	×	×	○	◎	△	×
II	×	◎	◎	×	×	×	×	×	△	△	×	×
III	○	◎	◎	○	○	×	×	×	○	◎	△	×
IV	△	◎	◎	◎	◎	◎	×	×	○	◎	△	△
V	△	◎	◎	◎	◎	◎	×	×	◎	◎	◎	△
VI	△	◎	◎	◎	◎	△	×	×	◎	◎	◎	△
VII	○	◎	◎	◎	◎	○	×	×	◎	◎	◎	△
VIII	×	◎	◎	◎	◎	×	×	×	◎	◎	○	△
IX	×	◎	◎	◎	◎	○	×	×	◎	◎	◎	○

◎: excellent, ○: good, △: poor, ×: very poor. Act: Acetone, DMAc: *N,N′*-dimethylacetamide, DMF: *N,N′*-dimethylformamide, DMSO: dimethyl sulfoxide, NMP: *N*-methyl-2-pyrrolidone, Py: Pyridine, THF: tetrahydrofuran. Tol: Toluene.

and methylene chloride (CH_2Cl_2), and in polar aprotic solvents including *N,N′*-dimethylacetamide (DMAc), *N,N′*-dimethylformamide (DMF), *N*-methyl-2-pyrrolidone (NMP), and tetrahydrofuran (THF).

Structures I–III showed the poorest solubility due to their simple aromatic frameworks and absence of solubilizing substituents. In particular, structures I and II incorporate $–CH_2–$ linkages within the main chain. While such alkyl segments may increase chain flexibility, they essentially function as hydrophobic moieties with negligible polarity. This structural feature is unfavorable when dissolution in polar solvents such as DMAc, DMF, or NMP is required. The presence of alkyl groups diminishes the extent of specific intermolecular interactions between the polymer chains and solvent molecules, including hydrogen bonding and dipole–dipole interactions, which are critical to achieving efficient solvation. Consequently, instead of enhancing solubility, the incorporation of $–CH_2–$ units suppresses polymer–solvent affinity, thereby leading to a marked reduction in overall solubility [52]. In contrast, Structures IV–IX demonstrated significantly improved solubility. This enhancement is attributed to the presence of bulky groups such as $–SO_2–$, $–CF_3$, and alkyl substituents, which increase free volume and reduce chain packing density, thereby facilitating solvent penetration [53, 54]. Specifically, Structures VIII and IX exhibited excellent solubility across multiple solvents, owing to the incorporation of voluminous $–C(CH_3)_2–$ (Structure VIII) and $–C(CF_3)_2–$ (Structure IX) substituents. These groups improve solvent–polymer interactions and enhance accessibility to solvent molecules.

4 Conclusions

In this study, a series of PAA precursors were synthesized by reacting nine different diamine monomers – each incorporating various substituents such as alkyl, ether (–O–), sulfone ($–SO_2–$), trifluoromethyl ($–CF_3$), and methyl ($–CH_3$) groups – with a dianhydride containing a flexible 1,4-butanediol unit in the polymer backbone. The resulting PAAs, composed of either *m*- or *p*-substituted structures, were converted into colorless and transparent polyimide (CPI) films via thermal imidization under controlled conditions. The thermomechanical, optical, and solubility properties of the CPI films were systematically investigated to understand the influence of diamine monomer structures.

The structure–property relationships of the synthesized CPIs revealed clear trends: CPI films with a high content of rigid and thermally stable aromatic structures demonstrated superior thermal and mechanical properties. In contrast, the introduction of bulky or electron-withdrawing substituents into the diamine units resulted in more distorted and flexible polymer backbones, leading to significantly improved optical transparency and solubility. Notably, the CPI films derived from relatively simple and slightly bent diamine structures exhibited excellent optical clarity, with YI values below 1 – comparable to that of conventional optical glass.

Overall, the nine newly developed CPI films exhibited the dual characteristics of high-performance engineering plastics and exceptional optical transparency. Moreover, their potential for scalable and cost-effective production highlights their suitability for diverse applications requiring both mechanical robustness and visual clarity, including flexible display substrates, solar panel coatings, and next-generation rollable or wearable electronic devices. These findings demonstrate that the CPIs reported in this work are promising candidates as polymeric alternatives to glass in advanced optoelectronic and flexible device technologies.

Acknowledgments: This research was supported by the Regional Innovation System & Education (RISE) program

through the Jeonbuk RISE Center, funded by the Ministry of Education (MOE) and the Jeonbuk State, Republic of Korea (2025-RISE-13-JJU).

Funding information: This research was supported by the Regional Innovation System & Education (RISE) program through the Jeonbuk RISE Center, funded by the Ministry of Education (MOE) and the Jeonbuk State, Republic of Korea (2025-RISE-13-JJU).

Author contributions: J.-H. Chang designed the project and wrote the manuscript. A.R. Lim reviewed and data analyzed. Y.S. Shin prepared the samples and participated in the data analysis. All authors have accepted responsibility for the entire content of this manuscript and approved its submission.

Conflict of interest: The authors state no conflict of interest.

Data availability statement: The datasets generated and/or analysed during the current study are available from the corresponding author on reasonable request.

References

1. Gouzman I, Grossman E, Verker R, Atar N, Bolker A, Eliaz N. Advances in polyimide-based materials for space applications. Adv Mater 2019;31: 1807738.
2. Chen Y, Liu Y, Min Y. Innovative polyimide modifications for aerospace and optoelectronic applications: synergistic enhancements in thermal, mechanical, and optical properties. ACS Appl Mater Interfaces 2025;17: 16016–26.
3. Jia C, Li Z, Wan Z, Jiang Z, Xue J, Shi J, et al. Ultra-thin perovskite solar cells with high specific power density based on colorless polyimide substrates. Nano Energy 2024;131:110259.
4. Wang Y, Chen Q, Zhang G, Xiao C, Wei Y, Li W. Ultrathin flexible transparent composite electrode via semi-embedding silver nanowires in a colorless polyimide for high-performance ultraflexible organic solar cells. ACS Appl Mater Interfaces 2022;14:5699–708.
5. Grabowska A, Fuentes Pineda R, Spinelli P, Soto Pérez G, Vinocour Pacheco FA, Babu V. Development of lightweight and flexible perovskite solar cells on ultrathin colorless polyimide foils. ACS Appl Mater Interfaces 2024;16:48676–84.
6. Li H, Li J, Chu W, Lin J, He P, Fan W. Ultrahigh absorption dominant EMI shielding polyimide composites with enhanced piezoelectric properties. Compos Sci Technol 2024;257:id. 110820.
7. Zhou L, Shen D, Gou P, He L, Xie F, He C, et al. Anisotropic high-strength polyimide-based electromagnetic interference shielding foam based on cation-π interaction. Chem Eng J 2023;477:id. 146992.
8. Rusu R-D, Constantin CP, Drobota M, Gradinaru LM, Butnaru M, Pislaru M. Polyimide films tailored by UV irradiation: surface evaluation and structure-properties relationship. Polym Degrad Stabil 2020;177:id. 109182.
9. Wu Z, He J, Yang H, Yang S. Progress in aromatic polyimide films for electronic applications: preparation structure and properties. Polymers 2022;14:id. 1269.
10. Zuo HT, Gan F, Dong J, Zhang P, Zhao X, Zhang QH. Highly transparent and colorless polyimide film with low dielectric constant by introducing meta-substituted structure and trifluoromethyl groups. Chin J Polym Sci 2021;39:455–64.
11. Wen Q, Tang A, Chen C, Liu Y, Xiao C, Tan J, et al. Impact of backbone amide substitution at the meta- and para- positions on the gas barrier properties of polyimide. Materials 2021;14:id. 2097.
12. Li B, Jiang S, Yu S, Chen Y, Tang X, Wu X, et al. Co-polyimide aerogel using aromatic monomers and aliphatic monomers as mixing diamines. J Sol Gel Sci Technol 2018;88:386–94.
13. Zhang H, Chen L, Xin H, Zhang J. Performance regulation and application evaluation of colorless polyimide for flexible displays. ACS Appl Mater Interfaces 2025;17:17358–67.
14. Zhu H, Su Y, Li J, Ding Y, Li M, Li W. Highly rigid and functional polyimides based on noncoplanar benzimidazolone diamines and their photolithography application. ACS Appl Polym Mater 2024;6:6130–9.
15. Pu C, Liu F, Xu H, Chen G, Tian G, Qi S, et al. Molecular dynamics study on the mechanism of poly(amic acid) chemical structure on thermal imidization process and polyimide architecture. Mater Today Chem 2023;33:id. 101679.
16. Ma P, Dai C, Liu H. High performance polyimide films containing benzimidazole moieties for thin film solar cells. E-Polymers 2019;19: 555–62.
17. Wu D, Yi C, Wang Y, Qi S, Yang B. Preparation and gas permeation of crown ether-containing co-polyimide with enhanced CO_2 selectivity. J Membr Sci 2018;551:191–203.
18. Kaya I, Kamaci M. Synthesis, optical, and thermal properties of polyimides containing flexible ether linkage. J Appl Polym Sci 2018;135: id. 46573.
19. Li H, Wang X, Gong Y, Zhao H, Liu Z, Tao L, et al. Polyimide/crown ether composite film with low dielectric constant and low dielectric loss for high signal transmission. RSC Adv 2023;13:7585–96.
20. Mushtaq N, Xing J, Li X, Chen G, Fang X. Synthesis and comparative study of high T_g and colorless polyamide – imides with different amide-to-imide ratio. J Polym Sci 2024;62:2014–26.
21. Novakov IA, Orlinson BS, Zavialov DV, Mednikov SV, Gurevich LM, Bogdanov AI, et al. A. Optically transparent (co) polyimides based on alicyclic diamines with improved dielectric properties. Russ Chem Bull 2023;72:1366–76.
22. Yu S, Zhou J, Xu A, Lao J, Luo H, Chen S. The scalable and high performance polyimide dielectrics containing alicyclic structures for high-temperature capacitive energy storage. Chem Eng J 2023;469:id. 13803.
23. Narzary BB, Baker BC, Yadav N, D'Elia V, Faul CF. Crosslinked porous polyimides: structure, properties and applications. Polym Chem 2021; 12:6494–514.
24. Zhuang Y, Seong JG, Lee YM. Polyimides containing aliphatic/alicyclic segments in the main chains. Prog Polym Sci 2019;92:35–88.
25. Wang W, Zhou G, Wang Y, Yan B, Sun B, Duan S, et al. Multiphotoconductance levels of the organic semiconductor of polyimide-based memristor induced by interface charges. J Phys Chem Lett 2022;13:9941–9.
26. Zhang T, Li P, Chen N, Su J, Yang Z, Wang D, et al. Flexible transparent layered metal oxides for organic devices. J Mater Chem C 2025;13: 9276–84.
27. Lu H, Yuan J, Chen Y, Xiang S, Lu Q. Super impact-resistant, high-strength, scratch-resistant, and foldable glass-like film for the next generation of ultra-thin flexible display. Flex Mat 2025;1:1–13.
28. Zhang H, Chen L, Xin H, Zhang J. Performance regulation and application evaluation of colorless polyimide for flexible displays. ACS Appl Mater Interfaces 2025;17:17358–67.

29. Wang X, Xu C, Wang C, Zhao X. Large π-Conjugated structure strategy for optimizing polyimide film-forming properties and developing gas fluorescence sensors. J Appl Polym Sci 2025;142:id. e56591.
30. Pavia DL, Lampman GM, Kriz GS. Introduction to spectroscopy. Saunders College Pub., New York, USA; 2008:14–95 pp. Chap. 2.
31. Pavia DL, Lampman GM, Kriz GS. Introduction to spectroscopy. Saunders College Pub., New York, USA; 2008:146-83 pp. Chap. 4.
32. Calosi M, D'Iorio A, Buratti E, Cortesi R, Franco S, Angelini R, et al. Preparation of high-solid PLA waterborne dispersions with PEG-PLA-PEG block copolymer as surfactant and their use as hydrophobic coating on paper. Prog Org Coating 2024;193:id. 108541.
33. Mushtaq N, Zhang Y, Nazir M, Tan L, Chen G, Fang X. Ultra-high T_g colorless polyimide film with balanced optical retardation and coefficient of thermal expansion for flexible display. Polymer 2025;321: id. 128085.
34. Zuo P, Li J, Chen D, Nie L, Gao L, Lin J, et al. Scalable co-cured polyimide/poly (p-phenylene benzobisoxazole) all-organic composites enabling improved energy storage density, low leakage current and long-term cycling stability. Mater Horiz 2024;11:271–82.
35. Yan C, Zhou J, Xu A, Long H, Luo H, Chen S. Sharply improved electrical insulation of polyimide dielectrics at elevated temperatures by charge reassignment engineering. Small 2025;21:id. 2501050.
36. Westwood MM, Schroeder BC. Solidifying the role of hydrogen bonds in conjugated polymers. J Mater Chem C 2024;12:19017–29.
37. Qingpei W, Thompson BC. Control of properties through hydrogen bonding interactions in conjugated polymers. Adv Sci 2024;11:id. e2305356.
38. Lee J, Kwak G. Extremely softened polyimides with long, branched alkyl side chains: shape memory characteristics and anticounterfeiting application. ACS Appl Polym Mater 2025;7:7526–34.
39. Feng J, Liu H, Yang S, Zhou Y, Zhang X, Wang X. Revealing molecular mechanisms of colorless transparent polyimide films with high thermal stability, superior mechanical and dielectric properties. Polymer 2023; 266:id. 125651.
40. Na Y, Kang S, Kwac LK, Kim HG, Chang JH. Monomer dependence of colorless and transparent polyimide films: thermomechanical properties, optical transparency, and solubility. ACS Omega 2024;9: 12195–203.
41. Sawada R, Yajima K, Takao A, Liu H, Ando S. Thermal, optical, and dielectric properties of bio-based polyimides derived from an isosorbide-containing dianhydride and diamines with long alkyl chains. J Photopolym Sci Technol 2024;37:507–16.
42. Zhang Z, Ren X, Huo G, Zhou X, Chen H, Zhang H, et al. Effect of free volume and hydrophilicity on dehumidification performance of 6FDA-Based polyimide membranes. J Membr Sci 2024;705:id. 122876.
43. Jia Y, Zhai L, Mo S, Liu Y, Liu LX, Du XY, et al. Effect of low-temperature imidization on properties and aggregation structures of polyimide films with different rigidity. Chin J Polym Sci 2024;42:1134–46.
44. Ran Z, Yang M, Wang R, Li J, Li M, Meng L, et al. Surface-gradient-structured polymer films with restricted thermal expansion for high-temperature capacitive energy storage. Energy Storage Mater 2025;74: id. 103952.
45. Zha JW, Wang F, Wan B. Polymer composites with high thermal conductivity: theory, simulation, structure and interfacial regulation. Prog Mater Sci 2024;148:id. 101362.
46. Sun Q, Tian K, Liu S, Zhu Q, Zheng S, Chen J, et al. A combination of "Inner-Outer skeleton" strategy to improve the mechanical properties and heat resistance of polyimide composite aerogels as composite sandwich structures for space vehicles. Compos Sci Technol 2024;252: id. 110620.
47. Kamalov A, Vaganov G, Simonova M, Kraft V, Nesterova A, Saprykina N, et al. Effect of the molar mass of polyimide based on pyromellitic dianhydride and 4, 4′-oxydianiline on dielectric and mechanical properties of nonwoven oriented polyimide materials. Polym Eng Sci 2024;64:2894–904.
48. Shi Y, Hu J, Li X, Jian J, Jiang L, Yin C, et al. High comprehensive properties of colorless transparent polyimide films derived from fluorine-containing and ether-containing dianhydride. RSC Adv 2024;14: 32613–23.
49. Na C, Kwac LK, Kim HG, Chang JH. Effect of organoclay on the physical properties of colorless and transparent copoly(amide imide) nanocomposites. RSC Adv 2024;14:9062–71.
50. Liu YY, Wang WK, Wu DY. Synthetic strategies for highly transparent and colorless polyimide film. J Appl Polym Sci 2022;139:id. e52604.
51. Yi C, Li W, Shi S, He K, Ma P, Chen M, et al. High-temperature-resistant and colorless polyimide: preparations, properties, and applications. Sol Energy 2020;195:340–54.
52. Mabesoone MFJ, MacLaren CJ, Weder C, Meijer EW. Solute–solvent interactions in modern physical organic chemistry. J Am Chem Soc 2020;142:17721–9.
53. Zhang H, Xiang Z, Fang P, Zang S, Zheng Z. Soluble polyimide-modified epoxy resin with enhanced comprehensive performances. J Appl Polym Sci 2025;142:id. e57400.
54. Zheng B, Li J, Li W, Zhang S, Lei H. Soluble photosensitive polyimide precursor with bisphenol A framework: synthesis and characterization. Polymers 2025;17:id. 1428.

Supplementary Material: This article contains supplementary material (https://doi.org/10.1515/rams-2025-0190).